

**Explosive spreading on complex networks: The role of synergy**Quan-Hui Liu,<sup>1,2</sup> Wei Wang,<sup>1,2,\*</sup> Ming Tang,<sup>1,2,†</sup> Tao Zhou,<sup>1,2</sup> and Ying-Cheng Lai<sup>3</sup><sup>1</sup>*Web Sciences Center, School of Computer Science and Engineering, University of Electronic Science and Technology of China, Chengdu 611731, China*<sup>2</sup>*Big Data Research Center, University of Electronic Science and Technology of China, Chengdu 611731, China*<sup>3</sup>*School of Electrical, Computer and Energy Engineering, Arizona State University, Tempe, Arizona 85287, USA*

(Received 6 April 2017; published 26 April 2017)

In spite of the vast literature on spreading dynamics on complex networks, the role of local synergy, i.e., the interaction of elements that when combined produce a total effect greater than the sum of the individual elements, has been studied but only for irreversible spreading dynamics. Reversible spreading dynamics are ubiquitous but their interplay with synergy has remained unknown. To fill this knowledge gap, we articulate a model to incorporate local synergistic effect into the classical susceptible-infected-susceptible process, in which the probability for a susceptible node to become infected through an infected neighbor is enhanced when the neighborhood of the latter contains a number of infected nodes. We derive master equations incorporating the synergistic effect, with predictions that agree well with the numerical results. A striking finding is that when a parameter characterizing the strength of the synergy reinforcement effect is above a critical value, the steady-state density of the infected nodes versus the basic transmission rate exhibits an explosively increasing behavior and a hysteresis loop emerges. In fact, increasing the synergy strength can promote the spreading and reduce the invasion and persistence thresholds of the hysteresis loop. A physical understanding of the synergy promoting explosive spreading and the associated hysteresis behavior can be obtained through a mean-field analysis.

DOI: [10.1103/PhysRevE.95.042320](https://doi.org/10.1103/PhysRevE.95.042320)**I. INTRODUCTION**

Disease or information spreading, a fundamental class of dynamical processes on complex networks [1–4], has been studied extensively in the past fifteen years [5–24]. Spreading dynamics can be classified into two types: irreversible and reversible. In an irreversible process, once an individual becomes infected, it cannot recover or return to the susceptible state, or, once an infected node recovers, it is immune to the same virus. Mathematically, irreversible spreading processes can be described by the susceptible-infected (SI), the susceptible-infected-recovered (SIR) [6], or the susceptible-exposed-infected-recovered (SEIR) model [10]. In contrast, in a reversible process, any node can be infected repeatedly in time, going through a cycle of susceptible and infected states. For example, in the infection process of tuberculosis and gonorrhea, an individual recovering from such a disease can be infected again with the same disease anytime. Mathematically, reversible spreading processes can be described by the susceptible-infected-susceptible (SIS) [5], the susceptible-infected-recovered-susceptible (SIRS) [25], or the susceptible-exposed-recovered-susceptible (SEIS) model [26]. One obvious result for both irreversible and reversible processes described by the classical SIR and SIS models, respectively, is that the fraction of infected nodes increases with the transmission rate continuously [4].

Recently, the reversible spreading dynamics is attracting much attention, especially in predicting the accurate theoretical epidemic thresholds. For the classical SIS model, a pioneering result was obtained through the heterogeneous mean-field (HMF) theory, which predicts a vanishing epidemic

threshold in scale-free networks with the power-law exponent  $\gamma \leq 3$  in the thermodynamic limit [5]. An improvement over HMF was given by the quenched mean-field (QMF) theory [27] considering the full network structure information, which gives the same result as the HMF theory for  $\gamma < 5/2$  and predicts a vanishing threshold when  $\gamma > 5/2$  in the thermodynamic limit. The threshold prediction of the QMF method is less convincing as the endemic state is caused by the local hub activation [28,29]. To elaborate the origin of this vanishing threshold, an analytical approach that captures the interplay between the lifetime of an infected hub and the time needed to infect a susceptible hub in the network was developed in Ref [30]. It provides strong analytical and numerical arguments that the threshold will vanish in any network with a degree distribution decaying slower than exponentially. Both the classical SIS model and the SIRS model were shown to have the same epidemic threshold predicted by the standard mean-field theories [25]. However, the effect of warning immunity exists in the SIRS model, which leads to collective activation with a finite threshold in scale-free networks for power-law exponent  $\gamma > 3$ , at odds with the QMF and qualitatively described by the HMF theory [31].

In this paper, we investigate the effect of synergy on the reversible spreading dynamics on complex networks. Synergy describes the situation where the interaction of elements that produce a total effect greater than the sum of individual elements when combined, i.e., the phenomenon commonly known as “one plus one is greater than two.” Intuitively, synergy should have a significant effect on the spreading dynamics. For example, in rumor or information spreading over a social network, a number of connected individuals possessing a piece of information make it more believable than just a single individual. Indeed, concrete evidence existed in both biological and social systems where the number of infected neighbors of a pair of infected-susceptible nodes would

\*wwzqbx@hotmail.com

†tangminghan007@gmail.com

enhance the transmission rate between them [32–35], such as fungal infection in soil-borne plant pathogens [34,35] where the probability for an infected node to affect its susceptible neighbors depends upon the number of other infected nodes connected to the infected node. In social systems, the synergistic effect was deemed important in phenomena such as the spread of adoption of healthy behavior [36,37], microblogging retweeting [38], opinion spreading and propagation [2,39], and animal invasion [40,41].

While the classic SIR and SIS models ignore the synergistic effect by assuming that the transmission of infection between a pair of infected-susceptible nodes is independent of the states of their neighbors, there were previous efforts to study the impact of synergy on irreversible spreading dynamics and its interplay with the network topology. In particular, threshold models [32,33,42] were developed, which take into account neighbors' synergistic effects on behavior spreading by assuming that a node adopts a behavior only when the number of its adopted neighbors is equal to or exceeds a certain adoption threshold. One result was that, for each node in the network with a fixed adoption threshold, the final adoption size tends to grow continuously and then decreases discontinuously when the mean degree of the network is increased. The SIR model was also generalized to modify the transmission rate between a pair of infected and susceptible nodes according to the synergistic effect [43–45], with the finding that it can affect the fraction of the epidemic outbreak, duration, and foraging strategy of spreaders. These existing works were exclusively for irreversible spreading dynamics. A systematic study to understand the impact of the synergistic effects on reversible spreading dynamics on complex networks is needed.

The goal of this paper is to investigate, analytically and numerically, the impacts of synergy on reversible spreading dynamics on complex networks. We first generalize the classic SIS model to quantify the effect of the number of infected neighbors connected to an infected node on the transmission rate between it and its susceptible neighbors. To characterize the impact on the steady state of the spreading dynamics, we consider the local nodal environment and derive the master equations (MEs) [46,47]. To gain a physical understanding, we assume that, statistically, nodes with the same degree have the same dynamical characteristics, so the mean-field approximation can be applied. Let  $\alpha$  be a parameter characterizing the strength of the synergistic effect. For random regular networks (RRNs), we find that for  $\alpha \geq \alpha_c$ , where  $\alpha_c$  is a critical value, a hysteresis loop [14,48] appears in which the steady-state infected density, denoted by  $\rho(\infty)$ , increases with the transmission rate  $\beta$  but typically exhibits an explosively increasing behavior, in contrast to the typical continuous transition observed in the classic SIS models [5]. For  $\alpha < \alpha_c$ , the hysteresis loop disappears and  $\rho(\infty)$  increases with  $\beta$  continuously. The phenomena of explosive spreading and hysteresis loop are general in that they also occur for complex networks of different topologies. Such as for synergistic irreversible spreading on SF networks, the hysteresis loop survives on networks of different power-law exponents in the thermodynamical limit.

Our paper is organized as follows. We describe the network model and the reversible spreading model in Sec. II, and the master equations and the mean-field approximation are used

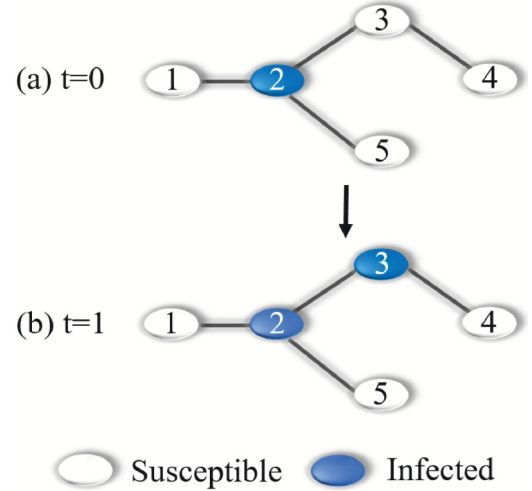


FIG. 1. Illustration of synergistic SIS spreading process on complex networks. (a) Initially (at  $t = 0$ ), node 2 is the seed and the remaining nodes are susceptible. Since there are no infected neighbors connected to node 2, it transmits the disease to one of its susceptible neighbors with probability  $p(0, \alpha) = \beta$ . (b) Node 3 is infected by node 2, which has not recovered. In this case, both nodes 2 and 3 have an infected neighbor and, at the next time step, they will infect one of their susceptible neighbors with a larger probability  $p(1, \alpha) \simeq (1 + \alpha)\beta$  due to the synergistic effect.

to analyze the spreading dynamics in Sec. III. The numerical verifications including the theory and the simulations are shown in Sec. IV. We briefly summarize our conclusions and prospects in Sec. V.

## II. MODEL

*Network model.* The networks in our study are generated from the uncorrelated configuration model [6] with degree distribution  $P(k)$ , where the degree-degree correlations can be neglected for large and sparse networks. Nodes in the network correspond to individuals or hosts responsible for spreading, with edges representing the interactions between nodal pairs.

*Model of reversible spreading dynamics.* We generalize the classic SIS model to incorporate the synergistic effect into the reversible spreading dynamics—we name it the synergistic SIS spreading model. At any time, each node can only be in one of two states: susceptible (S) or infected (I). An infected node can transmit the disease to its susceptible neighbors. The synergistic mechanism models the role of infected neighbors connected to a transmitter (i.e., an infected node) in enhancing the transmission probability. The synergistic SIS spreading process is illustrated schematically in Fig. 1. The synergistic reversible spread process is different from the core contact process in Ref. [49], in which a susceptible node is infected when at least  $k$  different infected neighbors of the node select the node for the infection, since the transmission rate between an infected node and a susceptible neighbor in the synergistic reversible spreading process changes with the number of infected neighbors connected to this infected node continuously. Besides, our model differs from the recent one in Ref. [50], which treated the synergistic effect

of ignorant individuals attached to a receiver (in ignorant state).

Initially, a fraction  $\rho_0$  of nodes is chosen as seeds (infected nodes) at random, while the remaining nodes are in the susceptible state. At time step  $t$ , each infected node transmits the disease to its susceptible neighbors with rate

$$p(m, \alpha) = 1 - (1 - \beta)^{1 + \alpha m}, \quad (1)$$

where  $m$  and  $\alpha$ , respectively, represent the number of the infected neighbors connected to the infected node and the strength of the synergistic effect, and  $\beta$  is the basic transmission rate in this paper. We use the synchronous updating method to simulate the spreading processes [27]. Thus, a susceptible node is infected by one of its infected neighbors with transmission probability  $p(m, \alpha)\Delta_t$  in each time step. In the same time step, all infected nodes recover to the susceptible state with recovery probability  $\mu\Delta_t$ , where  $\mu$  represents the recovery rate. Time is increased by  $\Delta_t = 1$ , and the dynamical process terminates when the system enters into the steady state (i.e., there is no infected node in the network or the number of infected nodes changes little with time). Equation (1) indicates that the larger the value of  $\alpha$  or  $m$ , the higher the rate  $p(m, \alpha)$  that an infected node will transmit the disease to its susceptible neighbor. Our model reduces to the classic SIS model for  $\alpha = 0$ . For  $\alpha > 0$  ( $\alpha < 0$ ), the synergistic effects are constructive (destructive) where the infected neighbors favor (hamper) transmission of the disease to the receivers. In our study, we consider only the constructive synergistic effect, where the infected neighbors of an infected node cooperate with it to spread the disease. In addition, we set  $\alpha \leq 1$  so that the synergistic ability of any infected neighbor of the infected node is less than that of itself. This assumption is based on consideration of real situations such as fungal infection in soil-borne plant pathogens where the probability for a susceptible node infected by a direct infected neighbor is always greater than that from an indirect infected neighbor [34,35].

### III. THEORY

We consider large and sparse networks with negligible degree-degree correlation. To develop the theory method and for the analysis, we assume the fraction of  $S$  ( $I$ ) state nodes is changed continuously with time. We first establish the master equations to describe the synergistic SIS spreading process quantitatively. We then provide an intuitive understanding of the role of synergy in the spreading dynamics through a mean-field analysis.

#### A. Master equations

In general, the transmission rate  $p(m, \alpha)$  between a pair of infected-susceptible nodes in the synergistic SIS spreading process is determined by the following three factors: (i) the basic transmission rate  $\beta$  between the pair of nodes, i.e., the rate in the absence of any synergistic effect; (ii) the number of infected neighbors connected to the infected node; and (iii) the strength  $\alpha$  of the synergistic effect. As there exists the strong dynamical correlation among the states of the neighboring nodes leading to the synergistic effect, the approach of master

equations [46,47] can be applied. For convenience, we denote  $S_{k,m}$  ( $I_{k,m}$ ) as the  $k$ -degree susceptible (infected) node with  $m$  infected neighbors and use  $s_{k,m}(t)$  and  $i_{k,m}(t)$  to express the fractions of  $S_{k,m}$  and  $I_{k,m}$  nodes at time  $t$ , respectively. The degree distribution and the average degree of the network are  $P_k$  and  $\langle k \rangle = \sum_k k' P_{k'}$ , respectively. The fraction of infected nodes with degree  $k$  at time  $t$  is given by

$$\rho_k(t) = \sum_{m=0}^k i_{k,m}(t) = 1 - \sum_{m=0}^k s_{k,m}(t),$$

and the total fraction of the infected nodes is  $\rho(t) = \langle \rho_k(t) \rangle \equiv \sum_k P_k \rho_k(t)$ .

To derive the master equations, it is necessary to obtain the probability for  $S_{k,m}$  to be infected. Initially,  $S_{k,m}$  has  $m$  infected neighbors so the probability for one of its infected neighbors to have degree  $k'$  is  $k' P_{k'} / \langle k \rangle$ . This degree  $k'$  infected neighbor of  $S_{k,m}$  may have zero, one, two, or up to  $k' - 1$  infected neighbors. The chance for the degree  $k'$  infected node to have  $n$  infected neighbors is  $i_{k',n}(t) / i_{k'}(t)$ , let  $\vartheta_{k'}(t) dt$  be the probability that this degree  $k'$  infected neighbor of  $S_{k,m}$  transmits the disease to  $S_{k,m}$ , therein,  $dt$  is an infinitesimally small time interval. Then the rate  $\vartheta_{k'}(t)$  can be written as

$$\vartheta_{k'}(t) = \sum_{n=0}^{k'-1} \frac{i_{k',n}(t)}{i_{k'}(t)} p(n, \alpha).$$

Let  $\pi_{k,m}(t) dt$  be the probability that the  $S_{k,m}$  node is being infected during the time interval  $[t, t + dt]$ . Since the  $S_{k,m}$  node has  $m$  infected neighbors, the rate  $\pi_{k,m}(t)$  can be written as

$$\pi_{k,m}(t) = m \sum_{k'} \frac{k' P_{k'}}{\langle k \rangle} \vartheta_{k'}(t). \quad (2)$$

There are three scenarios that can lead to an increase in  $s_{k,m}(t)$ : (i) recovery of  $I_{k,m}$  with rate  $\mu$ ; (ii) infection of a susceptible neighbor of  $S_{k,m-1}$ ; and (iii) recovery of an infected neighbor of  $S_{k,m+1}$ . The second (third) scenario corresponds to the situation where an S-S (S-I) edge changes into an S-I (S-S) edge, where an S-S edge connects two susceptible nodes, an S-I edge links a susceptible and an infected nodes, and so on. Denote  $\beta^s(t)$  as the rate that an S-S edge changes to S-I at time  $t$ . Then  $\beta^s(t) dt$  is the probability that an S-S edge changes into S-I in the time interval  $[t, t + dt]$ . To calculate  $\beta^s(t)$ , we can count the number of S-S edges [i.e.,  $\sum_k P_k \sum_{m=0}^k (k-m) s_{k,m}(t)$ ] in the network at time  $t$ , and then count the number of edges, which switches from being S-S edges to S-I edges [i.e.,  $\sum_k P_k \sum_{m=0}^k (k-m) s_{k,m}(t) \pi_{k,m}(t) dt$ ] in this time interval. We can approximate the probability  $\beta^s(t) dt$  as the ratio of edges that switches from being S-S to S-I in the time interval  $[t, t + dt]$ . The rate  $\beta^s$  can thus be approximated as

$$\beta^s(t) = \frac{\sum_k P_k \sum_{m=0}^k (k-m) \pi_{k,m}(t) s_{k,m}(t)}{\sum_k P_k \sum_{m=0}^k (k-m) s_{k,m}(t)}. \quad (3)$$

Since the probability for the recovery of an infected node does not depend on its neighbors, the probability that an S-I edge changes to S-S is  $\mu dt$ . Similarly, there are three cases leading to a decrease in  $s_{k,m}(t)$ :  $S_{k,m}$  being infected with probability  $\pi_{k,m}(t) dt$ ; infection of a susceptible neighbor of  $S_{k,m}$  with probability  $\beta^s(t) dt$ ; and recovery of an infected neighbor of

$s_{k,m}$  with probability  $\mu dt$ . We then obtain the time evolution equation of  $s_{k,m}(t)$  as

$$\begin{aligned} \frac{d}{dt}s_{k,m}(t) = & \mu i_{k,m}(t) + \beta^s(t)(k-m+1)s_{k,m-1}(t) \\ & + \mu(m+1)s_{k,m+1}(t) \\ & - [\pi_{k,m}(t) + \beta^s(t)(k-m) + \mu m]s_{k,m}(t). \end{aligned} \quad (4)$$

Analogously, we can derive the time evolution equation of  $i_{k,m}(t)$ :

$$\begin{aligned} \frac{d}{dt}i_{k,m}(t) = & \pi_{k,m}(t)s_{k,m}(t) + \beta^i(t)(k-m+1)i_{k,m-1}(t) \\ & + \mu(m+1)i_{k,m+1}(t) \\ & - [\mu + \beta^i(t)(k-m) + \mu m]i_{k,m}(t), \end{aligned} \quad (5)$$

where  $\beta^i(t)$  is the rate at which the edge S-I switches to I-I in the network at time  $t$ . The calculation method of  $\beta^i(t)$  is the same as the computation of  $\beta^s(t)$ . First, we count the number of S-I edges in the network at time  $t$ , i.e.,  $\sum P_k \sum_{m=0}^k m s_{k,m}(t)$ , then we count the number of edges that switch from being S-I edges to I-I edges in the time interval  $[t, t+dt]$ , i.e.,  $\sum P_k \sum_{m=0}^k m s_{k,m}(t) \pi_{k,m}(t) dt$ . Then the ratio between the latter and the former is the probability that an S-I edge changes into I-I edge. Additionally,  $\beta^i(t)$  can be approximately calculated as

$$\beta^i(t) = \frac{\sum P_k \sum_{m=0}^k m \pi_{k,m}(t) s_{k,m}(t)}{\sum P_k \sum_{m=0}^k m s_{k,m}(t)}. \quad (6)$$

If the initially infected nodes are distributed uniformly on the network, the initial conditions of Eqs. (2)–(6) are

$$\begin{aligned} s_{k,m}(0) &= [1 - \rho(0)] B_{k,m}[\rho(0)] \quad \text{and} \\ i_{k,m}(0) &= \rho(0) B_{k,m}[\rho(0)], \end{aligned}$$

where  $B_{k,m}(p) = \binom{k}{m} p^m (1-p)^{k-m}$ . Numerically solving Eqs. (2)–(6), we obtain the quantities  $i_{k,m}$  and  $s_{k,m}$  at any time  $t$ . The quantity  $\rho(\infty)$  can be calculated as  $\rho(\infty) = \sum_k P_k \sum_{m=0}^k i_{k,m}(\infty)$ , and we have  $s(\infty) = 1 - \rho(\infty)$ .

## B. Mean-field approximation

To gain physical insights into the role of synergistic effects in spreading dynamics, we develop a mean-field analysis. In particular, we assume that nodes with the same degree exhibit approximately identical dynamical behaviors. The time evolution of the fraction of the degree  $k$  infected nodes is then given by

$$\begin{aligned} \frac{d}{dt}\rho_k(t) = & [1 - \rho_k(t)]k \sum_{k'} \frac{k' P_{k'} \rho_{k'}}{\langle k \rangle} \\ & \times \sum_{m=0}^{k'-1} B_{k'-1,m}(w) p(m, \alpha) - \mu \rho_k(t), \end{aligned} \quad (7)$$

where  $w = \sum_k k P_k \rho_k / \langle k \rangle$  is the probability that one end of a randomly chosen edge is infected,  $\rho(t) = \sum_k P_k \rho_k(t)$ , and the fraction of susceptible nodes at time  $t$  is  $s(t) = 1 - \rho(t)$ . The

steady state of synergistic SIS process in Eq. (7) corresponds to the condition  $\frac{d}{dt}\rho_k(t) = 0$ . For degree  $k$  we have

$$\begin{aligned} \rho_k(\infty) = & \frac{[1 - \rho_k(\infty)]k}{\mu} \\ & \times \sum_{k'} \frac{k' P_{k'} \rho_{k'}(\infty)}{\langle k \rangle} \sum_{m=0}^{k'-1} B_{k'-1,m}(w) p(m, \alpha), \end{aligned} \quad (8)$$

which can be solved analytically for RRNs by approximating  $1 - (1 - \beta)^{(1+\alpha m)}$  as  $\beta(1 + \alpha m)$  for small  $\beta$ . We get

$$\begin{aligned} \rho(\infty) = & -\frac{\alpha \beta k(k-1)}{\mu} \rho(\infty)^3 + \frac{[\alpha \beta k(k-1) - \beta k]}{\mu} \rho(\infty)^2 \\ & + \frac{\beta k}{\mu} \rho(\infty), \end{aligned} \quad (9)$$

for  $t \rightarrow \infty$ . Solving Eq. (9), we get the infected density  $\rho(\infty)$ .

The epidemic threshold is a critical parameter value above which a global epidemic occurs but below which there is no epidemic. Similar to the analysis of the classic SIS spreading dynamics, we can obtain the critical condition from the nontrivial solution of Eq. (9). In particular, the function

$$\begin{aligned} g[\rho(\infty), \beta, \mu, \alpha] = & -\frac{\alpha \beta k(k-1)}{\mu} \rho(\infty)^3 \\ & + \frac{[\alpha \beta k(k-1) - \beta k]}{\mu} \rho(\infty)^2 \\ & + \frac{\beta k}{\mu} \rho(\infty) - \rho(\infty), \end{aligned} \quad (10)$$

becomes tangent to the horizontal axis at  $\rho_c(\infty)$ , which is the critical infected density in the limit  $t \rightarrow \infty$ . The critical condition is given by

$$\left. \frac{dg[\rho(\infty), \beta, \mu, \alpha]}{d\rho(\infty)} \right|_{\rho_c(\infty)} = 0. \quad (11)$$

Furthermore, the basic critical transmission rate can be calculated as:

$$\beta_c = \frac{\mu}{\Gamma}, \quad (12)$$

where

$$\Gamma = k[1 - 2(1 - (k-1)\alpha)\rho_c(\infty) - 3(k-1)\alpha\rho_c(\infty)^2].$$

Numerically solving Eqs. (9) and (12), we get the critical transmission rate  $\beta_c$ . For  $\alpha = 0$ , our synergistic SIS spreading model reduces to the classic SIS spreading model, and Eq. (9) has a trivial solution  $\rho(\infty) = 0$ . For  $\alpha = 0$ , Eq. (9) has only one nontrivial solution. We thus see that  $\rho(\infty)$  increases with  $\beta$  continuously. As shown in Fig. 2(a), the function  $g[\rho(\infty), \beta, \mu, \alpha]$  is tangent to the horizontal axis at  $\rho(\infty) = 0$ . Combining Eqs. (9) and (12), we obtain the continuous critical transmission rate  $\beta_c = \mu/k$  for  $\alpha = 0$ .

For  $\alpha > 0$  so synergistic effects exist,  $\rho(\infty) = 0$  is a trivial solution since Eq. (9) is a cubic equation for the variable  $\rho(\infty)$  without any constant term. As shown in Fig. 2(b), for a fixed  $\alpha > 0$  (e.g.,  $\alpha = 0.9$ ), the number of solutions of Eq. (9) is dependent upon  $\beta$ , and there exists a critical value of  $\beta$  at which Eq. (9) has three roots (fixed points), indicating the occurrence of a saddle-node bifurcation [51,52]. The bifurcation analysis of Eq. (9) reveals the physically meaningful stable solution of

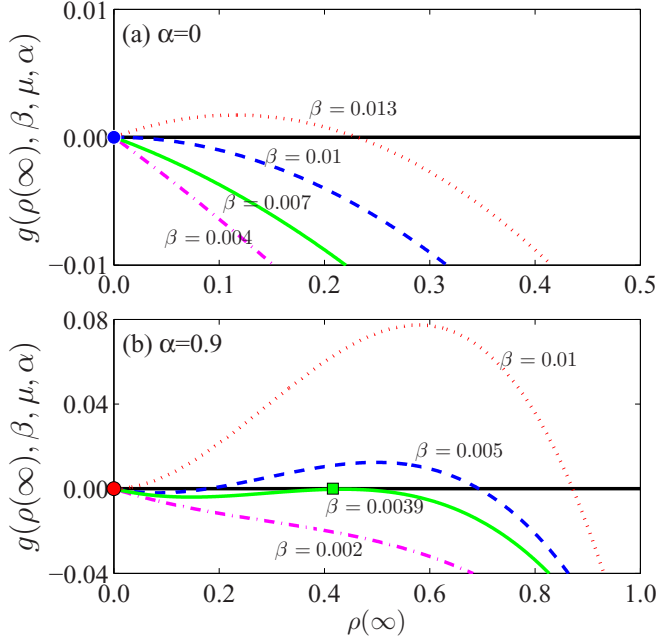


FIG. 2. Illustration of graphical solution of Eq. (10). For random regular networks with  $k = 10$ , (a) continuously increasing behavior of  $\rho(\infty)$  with  $\beta$  for  $\alpha = 0$ , (b) explosive change in  $\rho(\infty)$  for  $\alpha = 0.9$ . The blue dashed line is tangent to the horizontal axis at  $\rho(\infty) = 0$  (i.e., the blue circle) in (a). The red circle and green square, respectively, represent the points of tangency for the red dotted line and green solid line in (b). The recovery rate is  $\mu = 0.1$ .

$\rho(\infty)$  will suddenly increase to an alternate outcome. In this case, an explosive growth pattern of  $\rho(\infty)$  with  $\beta$  emerges. Also, whether the unstable state stabilizes to an outbreak state [ $\rho(\infty) > 0$ ] or an extinct state [ $\rho(\infty) = 0$ ] depends on the initial fraction of the infected seeds. As a result, a hysteresis loop emerges [14,48]. To distinguish the two thresholds of the hysteresis loop, we denote  $\beta_{inv}$  as the invasion threshold corresponding to the trivial solution [ $\rho(\infty) = 0$ ] of Eq. (9), associated with which the disease starts with a small initial fraction of the infected seeds, and let  $\beta_{per}$  be the persistence threshold corresponding to the nontrivial solution [ $\rho_c(\infty) > 0$ ] of Eq. (9), at which the disease starts with a higher initial fraction of the infected seeds [14,48]. Substituting the trivial solution [ $\rho(\infty) = 0$ ] into Eq. (12), we obtain the invasion threshold as

$$\beta_{inv} = \frac{\mu}{k}. \quad (13)$$

Note that the classic SIS spreading process has the same invasion threshold. We can also solve Eqs. (9) and (12) simultaneously to get the persistence threshold  $\beta_{per}$  with  $\rho_c(\infty) > 0$ .

We now present an explicit example to understand the relationship between  $\rho(\infty)$  and  $\beta$ . As shown in Fig. 2(b) for  $\alpha = 0.9$ , numerically solving Eqs. (9) and (12) gives the function  $g[\rho(\infty), \beta, \gamma, \alpha]$ , which becomes tangent to the horizontal axis for  $\beta_{inv} = 0.01$  or  $\beta_{per} \approx 0.0039$ . From Fig. 2(b), we see that Eq. (9) has three fixed points when  $\beta$  is in the range of  $(\beta_{inv}, \beta_{per})$ . As a result, the steady-state infection density depends on  $\rho_0$ . If the disease starts with

a small initial fraction of infected seeds, the root with the smallest value [ $\rho(\infty) = 0$ ] of Eq. (9) corresponds to the steady state. However, if the disease starts with a large initial fraction of infected seeds, the root with the largest value is the infected density in the steady state. When  $\beta$  is smaller than  $\beta_{per}$  or larger than  $\beta_{inv}$ , the initial fraction of infected seeds has no effect on the steady state.

Next, to determine the critical value of infected neighbors' synergy effects  $\alpha_c$ , across which the dependence of  $\rho(\infty)$  on  $\beta$  changes from being continuous (discontinuous) to discontinuous (continuous), we can numerically solve Eqs. (9) and (11) together with the condition [53]

$$\frac{d^2 g[\rho(\infty), \beta, \mu, \alpha]}{d\rho^2(\infty)} \Big|_{\rho_c(\infty)} = 0, \quad (14)$$

we obtain

$$\alpha_c = \frac{1}{k - 1 - 3(k - 1)\rho_c(\infty)}. \quad (15)$$

Combining Eqs. (9), (11), and (15), we get  $\alpha_c = 1/(k - 1)$ , which is dependent only on the degree of the RRNs.

#### IV. NUMERICAL VERIFICATION

We perform extensive simulations of synergistic SIS spreading processes on RRNs of size  $N = 10^4$  and degree  $k = 10$ . The synchronous updating spreading process is carried out as follows. At the beginning,  $\rho_0$  fraction of nodes are randomly selected as the initial infected nodes (i.e., seeds), and all other nodes are susceptible. In each time step, each susceptible node  $i$  becomes infected with probability  $\sum_{j \in N(i)} p(m_j, \alpha)$ , where  $N(i)$  is the set of infected neighbors of node  $i$  and  $m_j$  is the number of infected neighbors of infected node  $j$ . In the same time, all infected nodes recover with probability  $\mu$ . Time increases by  $\Delta_t = 1$ . To avoid the finite-size systems to enter into the absorbing state, we set  $t_{max} = 10^4$ , where the dynamical process terminates when there is no infected node in the network or the dynamical process iterates  $10^4$  steps. Finally, we average the number of infected nodes in the time step [9900, 10000] as the steady density of infected nodes in this realization.

To calculate the pertinent statistical averages we use 30 network realizations and at least  $10^3$  independent dynamical realizations for each parameter setting. To be concrete, we set the recovery rate as  $\mu = 0.1$  in all simulations, since more simulation results show that the results of synchronous updating method are very close to the asynchronous updating method when the recover rate and the time step of the synchronous updating method are set as  $\mu = 0.1$  and  $\Delta_t = 1$  [54,55] (also see the comparison in the Appendix). To obtain the numerical thresholds  $\beta_{inv}$  and  $\beta_{per}$ , we adopt the susceptibility measure [56]:

$$\chi = N \frac{\langle \rho(\infty)^2 \rangle - \langle \rho(\infty) \rangle^2}{\langle \rho(\infty) \rangle}, \quad (16)$$

where  $\rho(\infty)$  is the steady-state density of infected nodes. In general,  $\chi$  exhibits a maximum value at  $\beta_{inv}$  and  $\beta_{per}$  when the initial fraction of the infected seeds is relatively small and large, respectively. We define  $\beta_{inv}^s$  ( $\beta_{per}^s$ ) as the numerical predictions of invasive (persist) threshold.

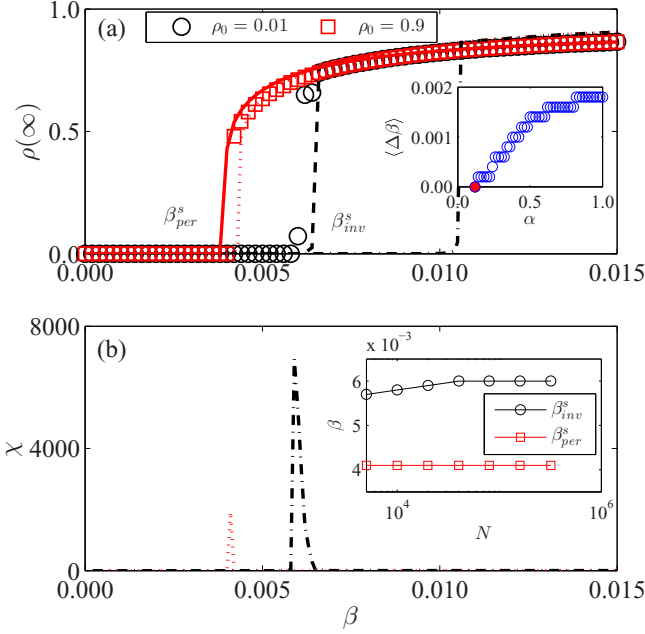


FIG. 3. Steady-state infected density  $\rho(\infty)$  and susceptibility measure  $\chi$  on random regular networks. (a) The density  $\rho(\infty)$  versus  $\beta$  for  $\alpha = 0.9$ , where the red squares and black circles are simulation results with initial infected density  $\rho_0 = 0.9$  and  $\rho_0 = 0.01$ , respectively. The red solid and black dashed lines are the results of master equations Eqs. (3)–(6) with the same respective initial seed fractions. The red dotted and black dotted dashed lines are results from the mean-field approximation [Eq. (11)] with the same respective initial seed fractions. The quantities  $\beta_{inv}^s$  and  $\beta_{per}^s$  are, respectively, the simulated invasion and persistence thresholds determined via the susceptibility measure. (b) Susceptibility measure  $\chi$  versus  $\beta$  with the same parameters as in (a). To discern the extremely small value of  $\chi$  for  $\rho_0 = 0.9$ , we plot the dotted line in (b) ten times larger than the original values. The inset in (a) shows the width of the hysteresis loop versus  $\alpha$ . The inset in (b) shows the thresholds (i.e.,  $\beta_{inv}^s$  and  $\beta_{per}^s$ ) versus size  $N$  of random regular network when  $\alpha = 0.9$ . Other parameters are  $\mu = 0.1$  and  $k = 10$ .

Figure 3(a) shows  $\rho(\infty)$  versus  $\beta$  for  $\alpha = 0.9$ , where the surprising phenomenon of explosive spreading, i.e.,  $\rho(\infty)$  exhibits an explosive increase as  $\beta$  passes through a critical point, can be seen, as predicted [Eqs. (2)–(6), and Eq. (9)]. In fact, there exists a range in  $\beta$ :  $[\beta_{inv}^s, \beta_{per}^s]$  in which the steady state depends on the value of  $\rho_0$ . In particular, the two different steady states correspond to the spreader-free state [ $\rho(\infty) = 0$ ] for an initially small fraction of infected seeds and the endemic state [ $\rho(\infty) > 0$ ] with initially larger fraction of infected nodes, respectively. The coexistence of endemic and spreader-free states, in the form of a hysteresis loop with explosive transitions between the states, is predicted by both theoretical approaches (i.e., the master equations and the mean-field theory), and is observed numerically. Figure 3(b) shows the susceptibility measure  $\chi$  versus  $\beta$  for the two cases of  $\rho_0 = 0.01$  and  $\rho_0 = 0.9$ . We see that the numerical thresholds  $\beta_{inv}^s$  and  $\beta_{per}^s$  determined through  $\chi$  match well with the predictions from the master equations, but the mean-field approximation gives only the value of  $\beta_{per}^s$  correctly. Letting  $\Delta\beta$  be the difference between  $\beta_{inv}^s$  and  $\beta_{per}^s$  (the width of the hysteresis loop), we find that  $\Delta\beta$  increases with  $\alpha$ , as shown in

the inset of Fig. 3(a), indicating that  $\beta_{inv}^s$  decreases faster than  $\beta_{per}^s$  as  $\alpha$  is increased. From the inset of Fig. 3(b), we know, with the increase of network size  $N$ ,  $\beta_{per}^s$  keeps unchanged and  $\beta_{inv}^s$  increases. The hysteresis loop becomes more visible and the simulation results are more close to the prediction results of the master equations. Thus, the hysteresis loop will survive in the thermodynamical limit.

To explain why the mean-field approximation can not accurately predict  $\beta_{inv}^s$ , and to give a qualitative explanation for the explosively increasing behavior of  $\rho(\infty)$  with  $\beta$ , we consider the case where the spreading process starts from a small fraction of infected seeds. Initially, for an infected seed [e.g., node 2 in Fig. 1(a)], all its neighbors are in the susceptible state. Thus, there is no synergistic effect when this infected node attempts to infect its susceptible neighbors. Also, the mean number of susceptible neighbors being infected by this infected node (without infected neighbors' synergy effect) before it recovers is  $R_0 = k \sum_{t=1}^{\infty} [(1-\mu)(1-p(0,\alpha))]^{t-1} p(0,\alpha)$  [54]. Therein,  $[(1-\mu)(1-p(0,\alpha))]^{t-1}$  is the probability that this infected node had not infected one of its susceptible neighbors and it had not recovered in  $t-1$  time steps, and  $p(0,\alpha)$  is the probability that this infected node infects one of its susceptible neighbor in the time step  $t$ .

Once the infected node ( $I_{k,0}$ ) has infected one of its susceptible neighbors [e.g., node 3 in Fig. 1(a)] successfully, the originally infected node becomes  $I_{k,1}$ , leading to a synergistic effect. In this case, compared with the case that the infected node is without infected neighbors' synergy effect, the mean number of susceptible neighbors being infected by this infected node before it recovers is increased by

$$\Delta_1 = (k-1) \sum_{t=2}^{\infty} [(1-\mu)(1-p(0,\alpha))]^{t-2} \times p(0,\alpha)(1-\mu)[p(1,\alpha) - p(0,\alpha)], \quad (17)$$

where the part  $\sum_{t=2}^{\infty} [(1-\mu)(1-p(0,\alpha))]^{t-2}$  means up to time step  $t-2$ , the original infected node had not infected a susceptible neighbor and had not recovered, and  $p(0,\alpha)(1-\mu)$  means at the  $(t-1)$ st time step this infected node infects a susceptible neighbor and does not recover. The increased transmission probability per edge is  $[p(1,\alpha) - p(0,\alpha)]$  and  $(k-1)$  means there are  $k-1$  susceptible neighbors left to be infected. Actually, once this infected node becomes  $I_{k,2}$  (with two infected neighbors), compared the  $I_{k,1}$  node, the mean number of susceptible neighbors being infected by this infected node before it recovers will be increased by  $\Delta_2$ . As we assume in the initial stage of the process,  $\Delta_n$  ( $n > 1$ ) is very tiny. If the average number of nodes infected by an infected node  $R \approx R_0 + \Delta_1$  is larger than 1, an epidemic may occur [4]. The average number of susceptible neighbors being infected by an infected node can be approximately calculated as  $R_0 + \Delta_1$ . Additionally, letting  $R_0 + \Delta_1 = 1$ , we can obtain the critical invasion threshold as

$$\beta_{inv}^s = \frac{\mu}{k + (k-1)(1-\mu)\alpha + \mu - 1}. \quad (18)$$

As shown in Fig. 4(a), the value of  $\beta_{inv}^s$  agrees well with the simulation invasion threshold  $\beta_{inv}^s$ . For the case of small initial infected density, the mean-field approximation fails to capture the dynamical correlation between the infected node and its

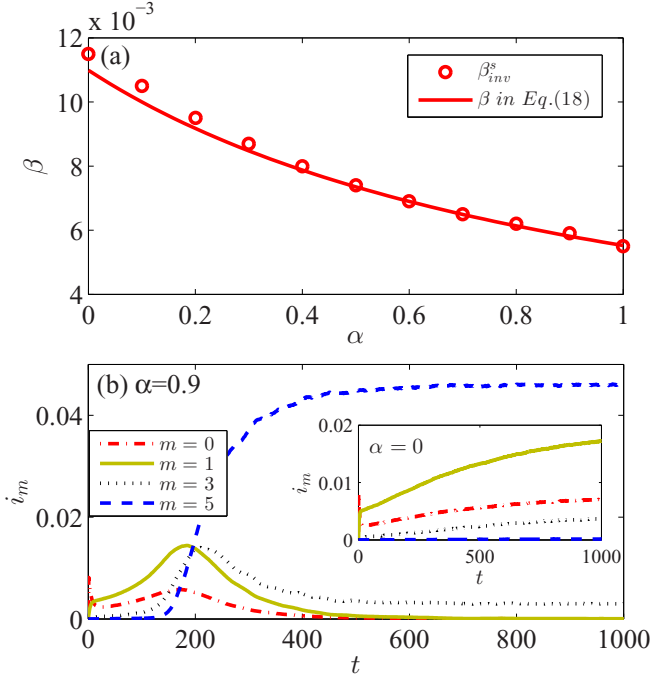


FIG. 4. Illustration the regime of explosive spreading. (a) Circles indicate the numerical predictions of invasive threshold  $\beta_{inv}^s$  in  $\alpha$ . The solid line shows the transmission rate  $\beta$  in Eq. (18). (b) The fraction  $i_m$  of infected nodes for different numbers of infected neighbors ( $m = 0, 1, 3, 5$ ) versus time  $t$  when the transmission rate is slightly larger than  $\beta_{inv}^s$ . (b) shows  $i_m$  versus  $t$  for  $\alpha = 0.9$  and  $\beta = 0.0064$  ( $\beta_{inv}^s = 0.0062$ ), where the inset shows the same plot for the classic SIS spreading dynamics for  $\beta = 0.0114$  ( $\beta_c = 0.0112$ ). Other parameters are  $\rho_0 = 0.01$ ,  $\mu = 0.1$ , and  $k = 10$ .

infected neighbors, which ignores that the synergy effect and leading to the derived invasion threshold is the same as the threshold in the classical SIS model.

To gain further insights into the cascading phenomenon and the explosive increase of  $\rho(\infty)$  with  $\beta$  for  $\alpha > \alpha_c$ , we calculate the fraction  $i_m$  of infected nodes with  $m$  ( $m = 0, 1, \dots, k$ ) infected neighbors versus time for  $\beta$  slightly larger than  $\beta_{inv}$  (for  $\alpha = 0.9$ ) and  $\beta_c$  (for  $\alpha = 0$ ). For  $\alpha < \alpha_c$  (e.g.,  $\alpha = 0$ ), the synergistic SIS spreading is reduced to the classic SIS dynamics. As shown in the inset of Fig. 4(b), for  $\beta \gtrsim \beta_c$  (e.g.,  $\beta = 0.0114$  and  $\beta_c = 0.0112$ ),  $i_m$  increases with  $t$  slowly and tends to a constant for large time. However, for  $\alpha = 0.9$ , if  $\beta \gtrsim \beta_{inv}^s$  (e.g.,  $\beta = 0.0064$  and  $\beta_{inv}^s = 0.0062$ ),  $i_m$  increases fast initially, reaches a peak at some small value of  $m$  (e.g.,  $m = 0, 1$ ), and then decreases rapidly [see Fig. 4(b)]. Due to the synergistic effect, even only one end of the I-I edge transmits the disease to its susceptible neighbors, the  $I_{k,1}$  node becomes  $I_{k,2}$ , which has a larger transmission rate than that from the original  $I_{k,1}$  node. As the spreading process continues, more susceptible nodes in the neighborhood of the infected node are infected so the  $I_{k,2}$  nodes become  $I_{k,3}$ ,  $I_{k,3}$  becomes  $I_{k,4}$ , and so on. For larger  $m$  values (e.g.,  $m = 3, 5$ ),  $i_m$  increases later and faster in reaching the peak, leading to a cascading process that results in explosive spreading. These provide an explanation for the continuously and relatively slowly increasing behavior

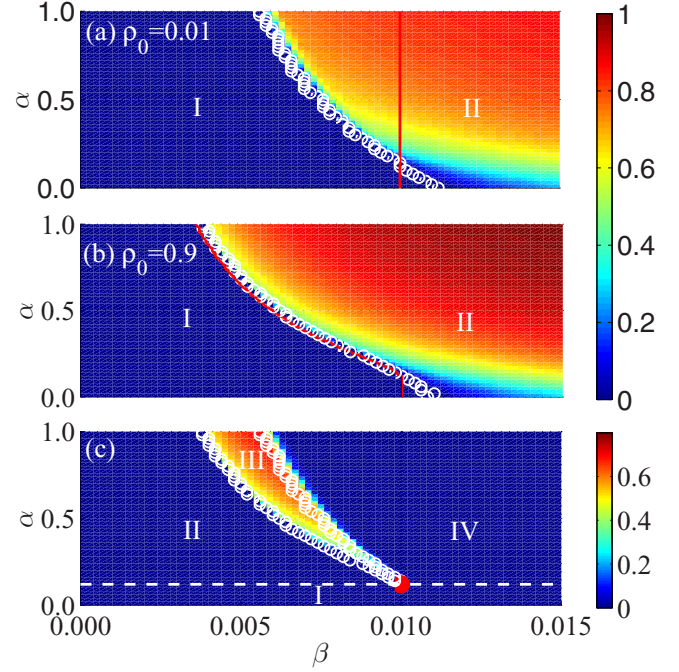


FIG. 5. Steady-state infected density  $\rho(\infty)$  and region of hysteresis in the parameter plane ( $\beta, \alpha$ ). (a), (b) For synergistic SIS spreading dynamics on random regular networks, color-coded values of  $\rho(\infty)$  in the parameter plane ( $\beta, \alpha$ ) for  $\rho_0 = 0.01$  and  $\rho_0 = 0.9$ , respectively. The numerically obtained invasion threshold  $\beta_{inv}^s$  and persistence threshold  $\beta_{per}^s$  (white circles) in (a) and (b), respectively, are determined by the susceptible measure  $\chi$ , and the corresponding theoretical values (red solid line) are from Eqs. (9) and (12). The persistence threshold predicted by the mean-field theory matches well with that from simulations, but there is disagreement for the invasion threshold, as shown in (a), (b), where I and II denote the parameter regions where the disease becomes extinct and an outbreak occurs, respectively. In (c), the color-coded values represent the difference between the values of  $\rho(\infty)$  in (b) and (a). There are four regions: in region I there is no hysteresis loop ( $\alpha < \alpha_c$ ); in region III there is a hysteresis behavior; and regions II and IV specify the borders of the hysteresis loop. Other parameters are  $\mu = 0.1$  and  $k = 10$ .

of  $\rho(\infty)$  for  $\alpha < \alpha_c$  and, more importantly, the explosively increasing behavior of  $\rho(\infty)$  with  $\beta$  for  $\alpha > \alpha_c$ .

From the above analysis, it can be obtained that both  $\beta$  and  $\alpha$  markedly affect  $\rho(\infty)$  and phase transition. Thus,  $\rho(\infty)$  and the phase transition on parameter plane ( $\beta, \alpha$ ) are further investigated in Fig. 5. Obviously,  $\rho(\infty)$  increases with  $\beta$  and  $\alpha$ , and the thresholds (i.e.,  $\beta_{inv}$  and  $\beta_{per}$ ) decreases with  $\alpha$  [See Figs. 5(a) and 5(b)]. A heuristic explanation for these results is that, due to the synergistic effect, there is an increase in the infection probability  $p(m, \alpha)$  between the infected nodes and their susceptible neighbors, thereby reducing the epidemic threshold (e.g.,  $\beta_{inv}$  and  $\beta_{per}$ ). Since the initial fraction of infected seeds impacts only the steady state associated with the region of the hysteresis loop, we can determine this region by computing the difference between the values of every point ( $\beta, \alpha$ ) in Figs. 5(b) and 5(a). As shown in Fig. 5(c), there are four regions. Only when  $\alpha$  is larger than a critical value  $\alpha_c$  [obtained from Eqs. (9), (11), and (15)] will the final density  $\rho(\infty)$  increase with  $\beta$  explosively (regions II, III, and IV) and

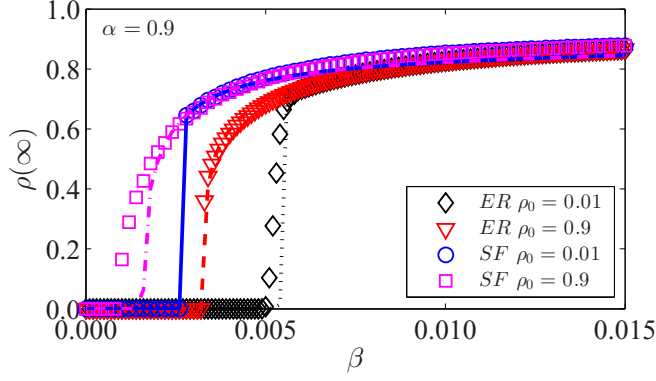


FIG. 6. Synergistic SIS spreading processes on random and scale-free networks. Steady-state simulation of infected nodes versus  $\beta$ , where symbols are results from simulation and the corresponding lines are predictions of the master equations Eqs. (3)–(6). The network parameters are  $N = 10^4$  and  $\langle k \rangle = 10$ .

a hysteresis loop appears (region III). Otherwise there is no hysteresis (region I). In region II, the disease becomes extinct, but there is an outbreak in region IV.

While we focus our study on RRNs for the reason that an understanding of explosive spreading can be obtained, the phenomenon can arise in general complex networks. To demonstrate this, we simulate synergistic spreading dynamics on Erdős-Rényi (ER) random and scale-free (SF) networks of size  $N = 10^4$  first. Figure 6 shows, for ER networks, an explosive increase in the steady-state infection density and a hysteresis loop with the parameter  $\beta$ . We also investigate the spreading dynamics on scale-free (SF) networks [6] constructed according to the standard configuration model [57]. The degree distribution is  $P(k) = \Gamma k^{-\gamma}$ , where  $\gamma$  is degree exponent and the coefficient is  $\Gamma = 1 / \sum_{k_{\min}}^{k_{\max}} k^{-\gamma}$  with the minimum degree  $k_{\min} = 3$ , maximum degree  $k_{\max} \sim N^{1/(\gamma-1)}$ , and  $\gamma = 3.0$ . The phenomena of explosive spreading and hysteresis loop are presented, as shown in Fig. 6. The theoretical predictions by master equations method match well with simulations.

We also implement the spreading processes on SF networks with different network sizes and different degree exponents, shown in Fig. 7. We find both the size of network and the power-law exponent will alter the invasion threshold and the persistence threshold. However, both of them will not impact the emergence of hysteresis loop, which means there exists a region of  $\beta$ , the steady-state infected density  $\rho(\infty)$  depends on the initial fraction of infected nodes. Further analysis also shows that the hysteresis loop will survive on the SF networks of different power-law exponents in the thermodynamical limit. The effects of degree heterogeneity on the synergistic spreading dynamics and a more accurate theoretical analysis method need to be further investigated.

## V. DISCUSSION

Synergy is a ubiquitous phenomenon in biological and social systems, and one is naturally curious about its effect on spreading dynamics on networks. There were previous works on synergistic irreversible spreading dynamics, and the

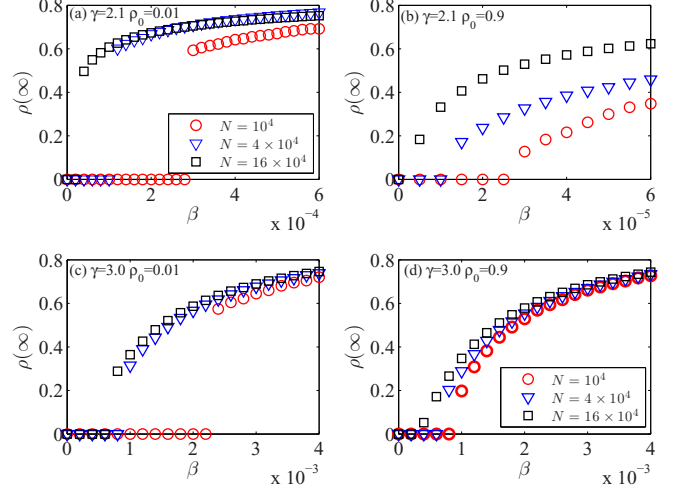


FIG. 7. The effects of degree heterogeneity and network size on the steady infected density  $\rho(\infty)$ . (a)  $\rho(\infty)$  versus  $\beta$  for  $\rho_0 = 0.01$  and (b) for  $\rho_0 = 0.9$  on the scale-free networks with degree exponent  $\gamma = 2.1$  of different network sizes. (c)  $\rho(\infty)$  versus  $\beta$  for  $\rho_0 = 0.01$  and (d) for  $\rho_0 = 0.9$  on the scale-free networks with degree exponent  $\gamma = 3.0$  of different network sizes. The average degree is fixed as  $\langle k \rangle = 10$ . The strength of synergy is  $\alpha = 0.9$ , and the recovery rate is  $\mu = 0.1$ .

goals of this paper are to construct and analyze a generic model for synergistic reversible spreading, where the effect of synergy is taken into account through enhancement in the transmission rate between an infected node and its susceptible neighbors. There are two factors determining the synergistic effect: the number of infected neighbors connected to the infected node that is to transmit the disease to one of its susceptible neighbors, and the strength of the synergistic reinforcement effect. For RRNs, the synergistic reversible spreading dynamics can be treated analytically by using the approach of master equations, as well as a mean-field approximation. Qualitatively, we find that synergy promotes spreading. The manner by which spreading is enhanced is, however, quite striking. In particular, if the strength is above a critical value that is solely determined by the degree of the network, there is an explosive outbreak of the disease in that the steady-state infection density increases abruptly and drastically as the basic transmission rate passes through a critical value. Associated with the explosive behavior is a hysteresis loop whereas, if the transmission rate is reduced through a different threshold, the final infected population collapses to zero. All these results have been obtained both analytically and numerically. While the analysis is feasible for RRNs, numerically we find that a similar explosive behavior occurs for general complex networks with a random or a scale-free topology. Especially, for synergistic irreversible spreading on SF networks, it finds that both the network size and the power-law exponent will alter the invasion threshold and persistence threshold, but it will not impact the emergence of hysteresis loop.

The main contributions of our work are thus the discovery of synergy-induced explosive outbreak for reversible spreading dynamics, and a qualitative and quantitative understanding

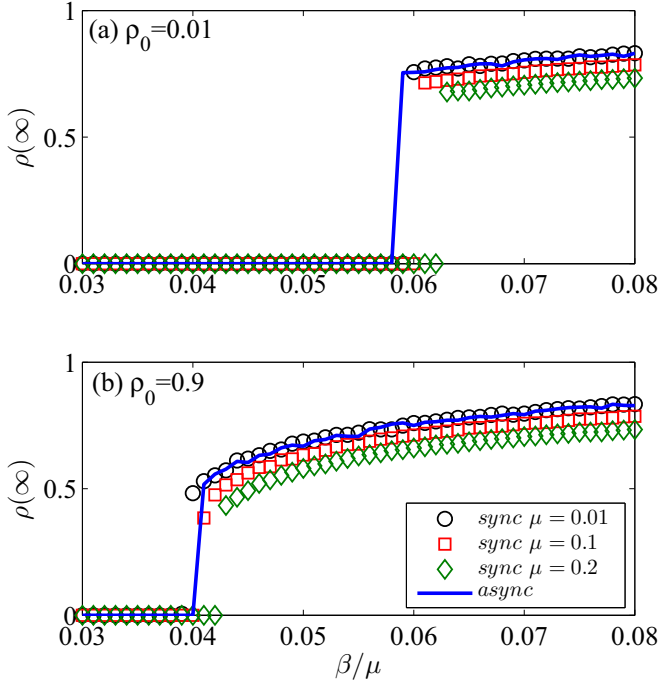


FIG. 8. The comparison between the simulation results of asynchronous updating method and synchronous updating with different recovery rates. The infected density  $\rho(\infty)$  in the steady state versus  $\beta/\mu$  for (a)  $\rho_0 = 0.01$  and (b)  $\rho_0 = 0.9$  on random regular networks with network size  $N = 10^4$  and average degree  $\langle k \rangle = 10$ . The strength of synergy is  $\alpha = 0.9$ . Therein, “async” means asynchronous updating and “sync” means synchronous updating.

of the phenomenon. A number of questions still remain. For example, the effects of network structural characteristics such as degree heterogeneity [3], clustering [58–60], community [61–63], and core periphery [64–67] on synergistic spreading dynamics need to be studied. Both an accurate theory method and the comparison of simulation results between the synchronous updating method and the asynchronous updating method are required. Finally, the study needs to be extended to more realistic networks such as multiplex networks [20,22,23,68], or temporal networks [69–71].

#### ACKNOWLEDGMENTS

This work was supported by the National Natural Science Foundation of China under Grants No. 11575041, No. 11105025, and No. 61433014, and the Fundamental Research Funds for the Central Universities (Grant No. ZYGX2015J153). Y.C.L. was supported by ARO under Grant No. W911NF-14-1-0504.

#### APPENDIX

We compare the simulation results of the asynchronous updating method and synchronous updating method [55]. For

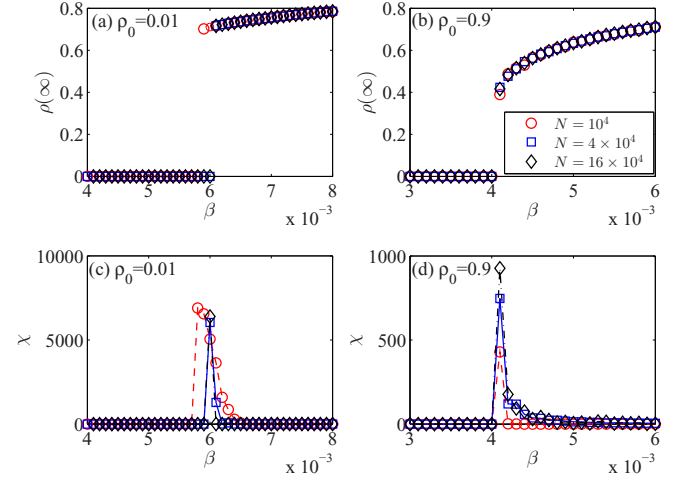


FIG. 9. Steady infected density  $\rho(\infty)$  and susceptibility measure  $\chi$  on random regular networks with different sizes. (a) The density  $\rho(\infty)$  versus  $\beta$  for  $\rho_0 = 0.01$  and (b) for  $\rho_0 = 0.9$ . The susceptibility measure  $\chi$  versus  $\beta$  for (c)  $\rho_0 = 0.01$  and (d)  $\rho_0 = 0.9$ . The values of  $\chi$  for  $N = 16 \times 10^4$  are divided by 10 in (c) and the values of  $\chi$  for  $N = 4 \times 10^4$  and  $N = 16 \times 10^4$  are multiplied by 100 in (d). Other parameters are set as  $\langle k \rangle = 10$ ,  $\alpha = 0.9$ , and  $\mu = 0.1$ .

the synchronous updating method, we use different recovery rates  $\mu = 0.01, 0.1$ , and  $0.2$ . As shown in Fig. 8, we find the simulation results with recovery rate  $\mu = 0.1$ , which we adopted in this paper, are very close to the simulation results of the asynchronous updating method. Both the explosive spreading phenomenon and the hysteresis loop also exist in the simulation results of asynchronous updating method, which means the updating method does not affect the conclusion of the paper qualitatively.

The finite-size analysis for random regular networks is also shown in Fig. 9, and some results are also presented in the inset of Fig. 3(b). It finds that the explosive spreading phenomenon and the hysteresis loop will survive in the thermodynamical limit.

For the asynchronous updating method: At any time  $t$ , we calculate each node’s transition rate  $\eta_i(t)$ . The rate for any susceptible node becoming infected is  $\eta_i(t) = \sum_{j \in N(i)} p(m_j, \alpha)$ , where  $N(i)$  is the set of infected neighbors of node  $i$  and  $m_j$  is the number of infected neighbors of infected node  $j$ . The rate for any infected node getting recovered is  $\eta_i(t) = \mu$ . Summing up all of them, we obtain the total transition rate  $a(t) = \sum_i \eta_i(t)$ . The time at which the next transition event occurs is  $t' = t + dt$ , where  $dt = 1/a(t)$ . The node chosen to change its state at time  $t'$  is sampled with a probability proportional to  $\eta_i(t)$ . That is, we generate a uniform number  $r \in [0, 1)$  and if  $\sum_{j=1}^{k-1} \eta_j(t)/a(t) < r < \sum_{j=1}^k \eta_j(t)/a(t)$ , then node  $k$  is chosen to change state. The whole process is iterated until the system reaches a stationary state, where either an absorbing state of all susceptible nodes arises or an endemic equilibrium is arrived (i.e., the number of infected nodes fluctuates stably in the long time limit).

[1] A. Barrat, M. Barthelemy, and A. Vespignani, *Dynamical Processes on Complex Networks* (Cambridge University Press, Cambridge, 2008).

[2] C. Castellano, S. Fortunato, and V. Loreto, *Rev. Mod. Phys.* **81**, 591 (2009).

- [3] M. E. J. Newman, *Networks: An Introduction* (Oxford University Press, Oxford, 2010).
- [4] R. Pastor-Satorras, C. Castellano, P. Van Mieghem, and A. Vespignani, *Rev. Mod. Phys.* **87**, 925 (2015).
- [5] R. Pastor-Satorras and A. Vespignani, *Phys. Rev. Lett.* **86**, 3200 (2001).
- [6] M. E. J. Newman, *Phys. Rev. E* **66**, 016128 (2002).
- [7] D. H. Zanette, *Phys. Rev. E* **65**, 041908 (2002).
- [8] Z. Liu, Y.-C. Lai, and N. Ye, *Phys. Rev. E* **67**, 031911 (2003).
- [9] M. Barthélemy, A. Barrat, R. Pastor-Satorras, and A. Vespignani, *Phys. Rev. Lett.* **92**, 178701 (2004).
- [10] M. Small and C. K. Tse, *Int. J. Bif. Chaos* **15**, 1745 (2005).
- [11] J. Zhou, Z. Liu, and B. Li, *Phys. Lett. A* **368**, 458 (2007).
- [12] R. Yang, L. Huang, and Y.-C. Lai, *Phys. Rev. E* **78**, 026111 (2008).
- [13] M. Tang, Z. Liu, and B. Li, *Europhys. Lett.* **87**, 18005 (2009).
- [14] T. Gross, C. J. D. D’Lima, and B. Blasius, *Phys. Rev. Lett.* **96**, 208701 (2006).
- [15] M. Kitsak, L. K. Gallos, S. Havlin, F. Liljeros, L. Muchnik, H. E. Stanley, and H. A. Makse, *Nat. Phys.* **6**, 888 (2010).
- [16] H.-X. Yang, W.-X. Wang, Y.-C. Lai, Y.-B. Xie, and B.-H. Wang, *Phys. Rev. E* **84**, 045101 (2011).
- [17] G.-H. Zhu, X.-C. Fu, and G.-R. Chen, *Appl. Math. Model.* **36**, 5808 (2012).
- [18] D. Brockmann and D. Helbing, *Science* **342**, 1337 (2013).
- [19] J. P. Gleeson, *Phys. Rev. X* **3**, 021004 (2013).
- [20] S. Boccaletti, G. Bianconi, and R. Criado, *Phys. Rep.* **544**, 1 (2014).
- [21] C. Granell, S. Gómez, and A. Arenas, *Phys. Rev. Lett.* **111**, 128701 (2013).
- [22] W. Wang, M. Tang, H. Yang, Y.-H. Do, Y.-C. Lai, and G. W. Lee, *Sci. Rep.* **4**, 5097 (2014).
- [23] Q. H. Liu, W. Wang, M. Tang, and H. F. Zhang, *Sci. Rep.* **6**, 25617 (2016).
- [24] W. Wang, M. Tang, H. E. Stanley, and L. A. Braunstein, *Rep. Prog. Phys.* **80**, 036603 (2017).
- [25] J.-D. Bancal and R. Pastor-Satorras, *Eur. Phys. J. B* **76**, 109 (2010).
- [26] N. Masuda and N. Konno, *J. Theor. Biol.* **243**, 64 (2006).
- [27] D. Chakrabarti, Y. Wang, C. Wang, J. Leskovec, and C. Faloutsos, *ACM T. Inform. Syst. Se.* **10**, 1 (2008).
- [28] A. V. Goltsev, S. N. Dorogovtsev, J. G. Oliveira, and J. F. F. Mendes, *Phys. Rev. Lett.* **109**, 128702 (2012).
- [29] H. K. Lee, P.-S. Shim, and J. D. Noh, *Phys. Rev. E* **87**, 062812 (2013).
- [30] M. Boguñá, C. Castellano, and R. Pastor-Satorras, *Phys. Rev. Lett.* **111**, 068701 (2013).
- [31] S. C. Ferreira, R. S. Sander, and R. Pastor-Satorras, *Phys. Rev. E* **93**, 032314 (2016).
- [32] M. Granovetter, *Ame. J. Soc.* **83**, 1420 (1978).
- [33] D. J. Watts, *Proc. Natl. Acad. Sci. USA* **99**, 5766 (2002).
- [34] J. L. Lockwood, *Ann. Rev. Phytopathol.* **26**, 93 (1988).
- [35] J. J. Ludlam, G. J. Gibson, W. Otten, and C. A. Gilligan, *J. Roy. Soc. Interface* **9**, 949 (2012).
- [36] D. Centola, *Science* **329**, 1194 (2010).
- [37] W. Wang, M. Tang, H.-F. Zhang, and Y.-C. Lai, *Phys. Rev. E* **92**, 012820 (2015).
- [38] N. O. Hodas and K. Lerman, *Sci. Rep.* **4**, 4343 (2014).
- [39] L. Lu, D.-B. Chen, and T. Zhou, *New J. Phys.* **13**, 123005 (2011).
- [40] J. D. Murray, *Mathematical Biology*, Vol. 17 of *Interdisciplinary Applied Mathematics*, 3rd ed. (Springer, Berlin, 2002).
- [41] D. M. Gordon, *Ant encounters: interaction networks and colony behavior* (Princeton University Press, Princeton, 2010).
- [42] J. Goldenberg, B. Libai, and E. Muller, *Mark. Lett.* **12**, 211 (2001).
- [43] F. J. Pérez-Reche, J. J. Ludlam, S. N. Taraskin, and C. A. Gilligan, *Phys. Rev. Lett.* **106**, 218701 (2011).
- [44] S. N. Taraskin and F. J. Pérez-Reche, *Phys. Rev. E* **88**, 062815 (2013).
- [45] D. Broder-Rodgers, F. J. Pérez-Reche, and S. N. Taraskin, *Phys. Rev. E* **92**, 062814 (2015).
- [46] J. Lindquist, J. Ma, P. Van den Driessche, and F. H. Willeboordse, *J. Math. Biol.* **62**, 143 (2011).
- [47] J. P. Gleeson, *Phys. Rev. Lett.* **107**, 068701 (2011).
- [48] H. Yang, M. Tang, and T. Gross, *Sci. Rep.* **5**, 13122 (2015).
- [49] H. Chae, S.-H. Yook, and Y. Kim, *New J. Phys.* **17**, 023039 (2015).
- [50] J. Gómez-Gardeñes, L. Lotero, S. Taraskin, and F. Pérez-Reche, *Sci. Rep.* **6**, 19767 (2016).
- [51] E. Ott, *Chaos in Dynamical Systems*, 2nd ed. (Cambridge University Press, Cambridge, 2002).
- [52] S. Strogatz, M. Friedman, A. J. Mallinckrodt *et al.*, *Comput. Phys.* **8**, 532 (1994).
- [53] G. J. Baxter, S. N. Dorogovtsev, A. V. Goltsev, and J. F. F. Mendes, *Phys. Rev. E* **82**, 011103 (2010).
- [54] P. Shu, W. Wang, M. Tang, P. Zhao, and Y.-C. Zhang, *Chaos* **26**, 063108 (2016).
- [55] P. G. Fennell, S. Melnik, and J. P. Gleeson, *Phys. Rev. E* **94**, 052125 (2016).
- [56] S. C. Ferreira, C. Castellano, and R. Pastor-Satorras, *Phys. Rev. E* **86**, 041125 (2012).
- [57] M. Catanzaro, M. Boguñá, and R. Pastor-Satorras, *Phys. Rev. E* **71**, 027103 (2005).
- [58] M. A. Serrano and M. Boguñá, *Phys. Rev. Lett.* **97**, 088701 (2006).
- [59] M. E. J. Newman, *Phys. Rev. Lett.* **103**, 058701 (2009).
- [60] A.-X. Cui, Z.-K. Zhang, M. Tang, P. M. Hui, and Y. Fu, *PLoS ONE* **7**, e50702 (2012).
- [61] M. Girvan and M. E. Newman, *Proc. Natl. Acad. Sci. USA* **99**, 7821 (2002).
- [62] S. Fortunato, *Phys. Rep.* **486**, 75 (2010).
- [63] K. Gong, M. Tang, P. M. Hui, H. F. Zhang, Y. Do, and Y.-C. Lai, *PLoS ONE* **8**, e83489 (2013).
- [64] S. P. Borgatti and M. G. Everett, *Soc. Net.* **21**, 375 (2000).
- [65] P. Holme, *Phys. Rev. E* **72**, 046111 (2005).
- [66] Y. Liu, M. Tang, T. Zhou, and Y. Do, *Sci. Rep.* **5**, 9602 (2015).
- [67] T. Verma, F. Russmann, N. Araújo, J. Nagler, and H. Herrmann, *Nat. Commun.* **7**, 10441 (2016).
- [68] M. Kivela, A. Arenas, M. Barthelemy, J. P. Gleeson, Y. Moreno, and M. A. Porter, *J. Complex Netw.* **2**, 203 (2014).
- [69] P. Holme and J. Saramäki, *Phys. Rep.* **519**, 97 (2012).
- [70] A. Barrat, B. Fernandez, K. K. Lin, and L.-S. Young, *Phys. Rev. Lett.* **110**, 158702 (2013).
- [71] A. Moinet, M. Starnini, and R. Pastor-Satorras, *Phys. Rev. Lett.* **114**, 108701 (2015).